

Phase and Intensity Control of Dissipative Kerr Cavity Solitons

Miro Erkintalo^{a,b}, Stuart G. Murdoch^{a,b} and Stéphane Coen^{a,b}

^aDepartment of Physics, The University of Auckland, Auckland 1010, New Zealand; ^bThe Dodd-Walls Centre for Photonic and Quantum Technologies, New Zealand

ARTICLE HISTORY

Compiled October 22, 2020

ABSTRACT

Dissipative Kerr cavity solitons are pulses of light that can persist in coherently driven nonlinear optical resonators. They have attracted significant attention over the past decade due to their rich nonlinear dynamics and key role in the generation of coherent microresonator optical frequency combs. Whilst the vast majority of implementations have relied on *homogeneous* continuous wave driving, the soliton’s “plasticity” combined with *inhomogeneous* driving offers attractive advantages for a host of applications. Here we review recent studies into the dynamics and applications of Kerr cavity solitons in the presence of inhomogeneous driving fields. In particular, we summarise the salient theoretical developments that allow for the analysis of CS motion in the presence of pump phase or amplitude inhomogeneities, and survey recent experiments that use pulsed driving to realise energy efficient and flexible microresonator optical frequency combs.

KEYWORDS

Cavity solitons; dissipative Kerr solitons; microresonator frequency combs; fibre ring resonators

1. Introduction

An externally-driven, passive optical resonator with Kerr nonlinearity can support persisting pulses of light known as temporal cavity solitons (CSs; also known as dissipative Kerr solitons) (Wabnitz 1993; Leo et al. 2010; Herr et al. 2014; Kippenberg et al. 2018). Such CSs are (typically ultrashort) pulses of light, sitting atop a low-level homogeneous background, and they can recirculate around the resonator indefinitely. They are attractors of the underlying nonlinear dynamical system, and their persistence is underpinned by a double-balance (Akhmediev and Ankiewicz 2008): all the energy they lose is replenished via parametric gain from the background on top of which they sit (and that is externally replenished by the driving field) and their dispersive spreading is cancelled by the self-focussing Kerr nonlinearity.

Analogous to spatial localized structures that can manifest themselves in diffractive resonators (Barland et al. 2002; Ackemann et al. 2009), temporal CSs were first observed in a macroscopic optical fibre ring resonator (Leo et al. 2010) and soon thereafter in a monolithic microresonator (Herr et al. 2014). The former (macroscopic) systems have proven invaluable for the controlled exploration of the characteristics and rich nonlinear dynamics of CSs (Leo et al. 2013; Anderson et al. 2016, 2017; Wang et al.

2018a; Nielsen et al. 2019; Xue et al. 2019), but it is the latter (microscopic) systems that have unleashed the solitons’ application potential (Kippenberg et al. 2018; Pasquazi et al. 2018). In particular, it is now well-understood that temporal CSs represent the time-domain counterparts of the coherent optical frequency combs that can be generated in Kerr nonlinear microresonators (Herr et al. 2014; Brasch et al. 2016; Yi et al. 2015; Joshi et al. 2016; Jang et al. 2018). Such soliton microresonator frequency combs represent one of the most important optical technologies to emerge in the past decade, with demonstrated applications including high-speed telecommunications (Marin-Palomo et al. 2017), optical distance measurements (Trocha et al. 2018; Suh and Vahala 2018; Riemensberger et al. 2020), high-resolution spectroscopy (Suh et al. 2016; Dutt et al. 2018; Lucas et al. 2018; Spencer et al. 2018), and detection of extrasolar planets (Suh et al. 2019; Obrzud et al. 2019).

Most CS systems use purely homogeneous, continuous wave (CW) laser radiation to drive the resonator [see Fig. 1(a)]. Whilst simple to implement, CW driving suffers from certain shortcomings (Obrzud et al. 2017; Xu et al. 2020b). First, CW driving fills the entire cavity with a homogeneous “holding” field, yet CSs only extract energy from the portion of the field with which they overlap. As the duration of that portion typically corresponds to a very small fraction of the cavity round trip time, a considerable amount of energy is effectively wasted, resulting in poor pump-to-soliton conversion efficiency (Bao et al. 2014; Xue et al. 2017). Second, with pure CW driving, it can be challenging (albeit not impossible) to control the specific soliton configuration that circulates in the resonator (Guo et al. 2017), making it in particular difficult to reach the single-soliton state that is arguably of most applied interest. Third, CW driving does not provide an intrinsic means to lock the soliton repetition rate to an external radiofrequency (RF) reference, which is needed for many applications.

The issues listed above have stimulated increasing interest in driving scenarios that go beyond the simplest paradigm of pure CW driving [see Fig. 1(b)]. In particular, it is now known that the introduction of phase or amplitude inhomogeneities on the cavity driving field allows CSs to be robustly trapped at specific temporal positions (Jang et al. 2015; Obrzud et al. 2017; Hendry et al. 2018; Cole et al. 2018), thus permitting control over the soliton configuration as well as their repetition rate. Moreover, the use of a pulsed driving source that is synchronised with the cavity round trip time has been shown to provide an attractive route to enhancing the pump-to-soliton conversion efficiency (Obrzud et al. 2017), and also to enable CS comb generation in resonators that would not be suitable under CW driving (Lilienfein et al. 2019; Xu et al. 2020b).

Here we review recent studies of CS dynamics in the presence of driving field inhomogeneities. In particular, we recount the key steps of a comprehensive theoretical description by Maggipinto et al. to elucidate the motion (or lack thereof) of CSs in the presence of phase or amplitude inhomogeneities (Maggipinto et al. 2000); describe how the appropriate CS drift velocities can be calculated in practice (Hendry et al. 2018); and survey recent experimental results.

2. Theory of CS motion

We begin by recalling the theory of CS motion under inhomogeneous driving fields. Whilst we focus on *temporal* CSs in *dispersive* resonators, our analysis follows closely the work of Maggipinto et al. that was originally presented in the context of *spatial* CSs in *diffractive* semiconductor microcavities (Maggipinto et al. 2000). We must also emphasise that, whilst our focus is on *external* inhomogeneities arising from the cavity

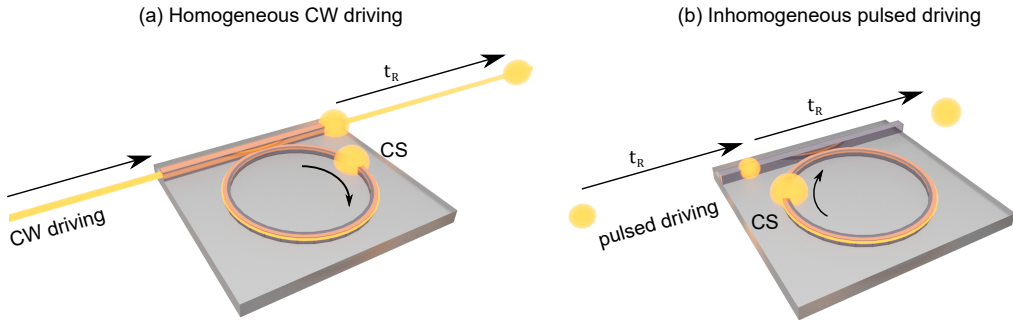


Figure 1. Schematic illustration of CS-supporting nonlinear resonator systems with (a) homogeneous CW and (b) inhomogeneous pulsed driving. In (a), a CW driving field produces a periodic train of ultrashort CS pulses that repeat at the cavity round trip time t_R . In (b), a pulsed driving field with periodicity t_R synchronously drives the resonator and produces intense ultrashort CS pulses with the same periodicity.

driving fields, the general theory presented below can also be extended to *internal* perturbations (Maggiolino et al. 2000) that underpin, e.g., the formation of bound soliton states (Wang et al. 2017) and soliton crystals (Cole et al. 2018; Karpov et al. 2019).

It is well known that the dynamics of temporal CSs in dispersive Kerr resonators can be described by the mean-field Lugiato-Lefever equation (Lugiato and Lefever 1987), which was first derived in the context of dispersive resonators by Haelterman et al. (Haelterman et al. 1992). In dimensionless form [see e.g. (Leo et al. 2010) for normalisation], and assuming anomalous dispersion, the equation reads:

$$\frac{\partial E}{\partial t} = \left[-1 + i(|E|^2 - \Delta) + i \frac{\partial^2}{\partial \tau^2} \right] E + S(\tau). \quad (1)$$

Here $E \equiv E(t, \tau)$ is the slowly-varying envelope of the electric field in the resonator, t is a slow time variable that describes the evolution of the field envelope over consecutive round trips, and τ is a fast time variable that describes the envelope's profile over a single round trip. The terms on the right-hand-side of Eq. (1) respectively describe cavity losses, Kerr nonlinearity, detuning between the driving field and the closest cavity resonance (Δ is the detuning normalised to the resonance half-width), anomalous group-velocity dispersion and coherent driving, with $S(\tau)$ the envelope of the driving field. For CW driving, $S(\tau) \equiv S_0$ where S_0 is a constant scalar; the presence of driving field inhomogeneities is in contrast described by a driving field with explicit fast time (τ) dependence.

The model described by Eq. (1) can be understood to consist of two real coupled partial differential equations (PDEs) that describe the evolution of the the real ($E_r = \text{Re}[E]$) and imaginary ($E_i = \text{Im}[E]$) components of the field envelope. To understand how CSs react to driving field inhomogeneities, we first find the steady-state ($\partial E(t, \tau)/\partial t = 0$) CS solutions of the model with homogeneous driving, $S(\tau) = S_0$. To this end, we use a multivariate Newton's method [see e.g. (Kelley 2003)], where the fast time is discretized into N elements and the partial derivatives $\partial^2/\partial \tau^2$ computed at each grid point to transform Eq. (1) into $2N$ real, coupled, ordinary differential equations (the factor of 2 comes from separation into real and imaginary parts). The

system of equations can be written succinctly as

$$\frac{\partial \mathbf{E}}{\partial t} = \mathbf{f}(\mathbf{E}), \quad (2)$$

where the discretized vector $\mathbf{E} \in \mathbb{R}^{2N}$ contains both the real and imaginary components of the field envelope computed at all the grid points and $\mathbf{f} : \mathbb{R}^{2N} \rightarrow \mathbb{R}^{2N}$ is a vector-valued function that represents the right-hand-side of Eq. (1). Newton's method iteratively finds the approximate solution to the system of equations $\mathbf{f}(\mathbf{E}) = \mathbf{0}$ and hence the approximate steady-state solution of Eq. (1). Starting from a suitable initial guess $\mathbf{E}^{(0)}$, the vector-valued function \mathbf{f} is approximated in the vicinity of the initial guess as the linearization

$$\mathbf{f}(\mathbf{E}) \approx \mathbf{f}(\mathbf{E}^{(0)}) + \mathbf{J}_f(\mathbf{E}^{(0)}) [\mathbf{E} - \mathbf{E}^{(0)}], \quad (3)$$

where $\mathbf{J}_f(\mathbf{E}^{(0)})$ is the Jacobian matrix of $\mathbf{f}(\mathbf{E})$ evaluated at $\mathbf{E}^{(0)}$. An improved approximation for the solution is then obtained by solving for the root of the right-hand-side of Eq. (3), yielding $\mathbf{E}^{(1)} = \mathbf{E}^{(0)} - [\mathbf{J}_f(\mathbf{E}^{(0)})]^{-1} \mathbf{f}(\mathbf{E}^{(0)})$. This procedure is then iteratively repeated until the solution converges to \mathbf{E}_s for which $\mathbf{f}(\mathbf{E}_s) \approx 0$.

Once the approximate steady-state solution \mathbf{E}_s is found, the eigenvalues and eigenvectors of the Jacobian matrix $\mathbf{J}_f(\mathbf{E}_s)$ provide information on the stability of the solution. In particular, the solution is dynamically stable only if none of the eigenvalues have a positive real part. Because of the translational symmetry of the system, there is always one eigenvector with zero eigenvalue; this corresponds to a *neutral* (or Goldstone) mode and its existence reflects the fact that, for the case of homogeneous driving [$S(\tau) = S_0$], CSs can occupy any position along the fast time axis.

The neutral mode underpins the fact that CSs can experience time-domain motion when subject to inhomogeneous driving fields (or other forms of inhomogeneities). Considering a steady-state solution \mathbf{E}_s with a CS centred at some temporal position τ_0 , we may write an inhomogeneous driving field as $S(\tau) = S_0 + P(\tau)$, where $S_0 \equiv S(\tau_0)$ is the local driving field amplitude at the CS position and $P(\tau)$ is a (possibly complex) continuous function that represents the inhomogeneity. (Note that $P(\tau_0) = 0$ by definition.) The CS then obeys the perturbed LLE, which can be discretized into the system of equations

$$\frac{\partial \mathbf{E}}{\partial t} = \mathbf{f}(\mathbf{E}) + \mathbf{P}, \quad (4)$$

where the vector $\mathbf{P} \in \mathbb{R}^{2N}$ contains both the real and imaginary components of $P(\tau)$ at all the grid points along fast time τ . Assuming that the perturbation amplitude and its variations are small in the vicinity of the CS, it can be shown (Maggipinto et al. 2000) that the soliton will experience time-domain drift at a rate given by

$$v = \frac{d\tau_0}{dt} = \frac{\langle \mathbf{v}_0 | \mathbf{P} \rangle}{\left\langle \mathbf{v}_0 \left| \frac{d\mathbf{E}_s}{d\tau} \right. \right\rangle}, \quad (5)$$

where $\mathbf{v}_0 \in \mathbb{R}^{2N}$ is the left-eigenvector with zero eigenvalue of the Jacobian matrix

evaluated at \mathbf{E}_s , that is, $[\mathbf{J}_f(\mathbf{E}_s)]^T \mathbf{v}_0 = 0$, and the inner product $\langle \mathbf{v}_0 | \mathbf{P} \rangle \in \mathbb{R}$ represents a vector dot product between \mathbf{v}_0 and \mathbf{P} . The numerator of Eq. (5) shows that the CS drift velocity is governed by the projection of the perturbation \mathbf{P} on the neutral mode (here described by \mathbf{v}_0). Recasting the discretized vectors into continuous functions so as to facilitate the analyses that will follow, we write the drift velocity as

$$v = \frac{d\tau_0}{dt} = \frac{\langle v_{0r}(\tau) | P_r(\tau) \rangle + \langle v_{0i}(\tau) | P_i(\tau) \rangle}{\left\langle v_{0r} \left| \frac{dE_{sr}}{d\tau} \right. \right\rangle + \left\langle v_{0i} \left| \frac{dE_{si}}{d\tau} \right. \right\rangle}, \quad (6)$$

where the subscripts r and i refer to real and imaginary parts and the inner product now represents an integration over fast time τ .

Equations (5) and (6) allow the CS drift velocity to be computed for arbitrary inhomogeneities $P(\tau)$. Here, one first finds the steady-state CS solution for a homogeneous driving amplitude S_0 using Newton's method, then computes the left eigenvectors \mathbf{v}_0 of the Jacobian with zero eigenvalue, and finally evaluates the inner product to find the velocity. In what follows, we review the drift velocities that are predicted for the case of pure phase and amplitude inhomogeneity, respectively.

2.1. Phase modulation

For a CW driving field with pure phase modulation, we have $S(\tau) = S_0 \exp[i\phi(\tau)]$, where $\phi(\tau)$ is a fast-time-dependent phase profile. Before using the normal mode theory outlined above, we note that a straightforward change of variables $E = E' \exp[i\phi(\tau)]$ in Eq. (1) predicts a CS drift velocity $v_{\text{PM}} = 2\phi'(\tau_0)$, where τ_0 is the position of the CS and $\phi'(\tau) = d\phi/d\tau$ (Firth and Scroggie 1996). This same result can also be derived from simple physical arguments based on an instantaneous frequency shift caused by the time-varying phase profile $\phi(\tau)$ (Jang et al. 2015); this latter approach further highlights the linear origins of CS drift due to phase perturbations. For the sake of completeness (and as a test of the validity of the normal mode theory), we now proceed to compute the drift velocity using Eqs. (5) and (6).

Without loss of generality, we can assume $\phi(\tau_0) = 0$ at the CS position τ_0 . Accordingly, in the vicinity of the soliton, we may approximate $S(\tau) \approx S_0[1 + i\phi(\tau)] = S_0 + iS_0\phi(\tau)$. The perturbation $P(\tau)$ is therefore purely imaginary, with $P_i(\tau) = S_0\phi(\tau)$. Expanding $\phi(\tau)$ as a Taylor series around the soliton, $\phi(\tau) \approx \phi'(\tau_0)(\tau - \tau_0)$ where $\phi'(\tau) = d\phi/d\tau$, substitution of this expression into Eq. (6) yields:

$$v_{\text{PM}} = \frac{d\tau_0}{dt} = a_{\text{PM}}(\Delta, S_0)\phi'(\tau_0), \quad (7)$$

where the coefficient $a_{\text{PM}}(\Delta, S_0)$ is given by

$$a_{\text{PM}}(\Delta, S_0) = S_0 \frac{\langle v_{0i}(\tau - \tau_0) | \tau - \tau_0 \rangle}{\left\langle v_{0r} \left| \frac{dE_{sr}}{d\tau} \right. \right\rangle + \left\langle v_{0i} \left| \frac{dE_{si}}{d\tau} \right. \right\rangle}, \quad (8)$$

where we used $\tau - \tau_0$ as the argument for v_{0i} to highlight that the neutral mode is centred at the CS position τ_0 . Note also the multiplicative prefactor S_0 .

Figure 2(a) shows the coefficient $a_{\text{PM}}(\Delta, S_0)$ as computed for a range of detunings Δ and driving amplitudes S_0 using Eq. (8). As can be seen, the coefficient a_{PM} as-

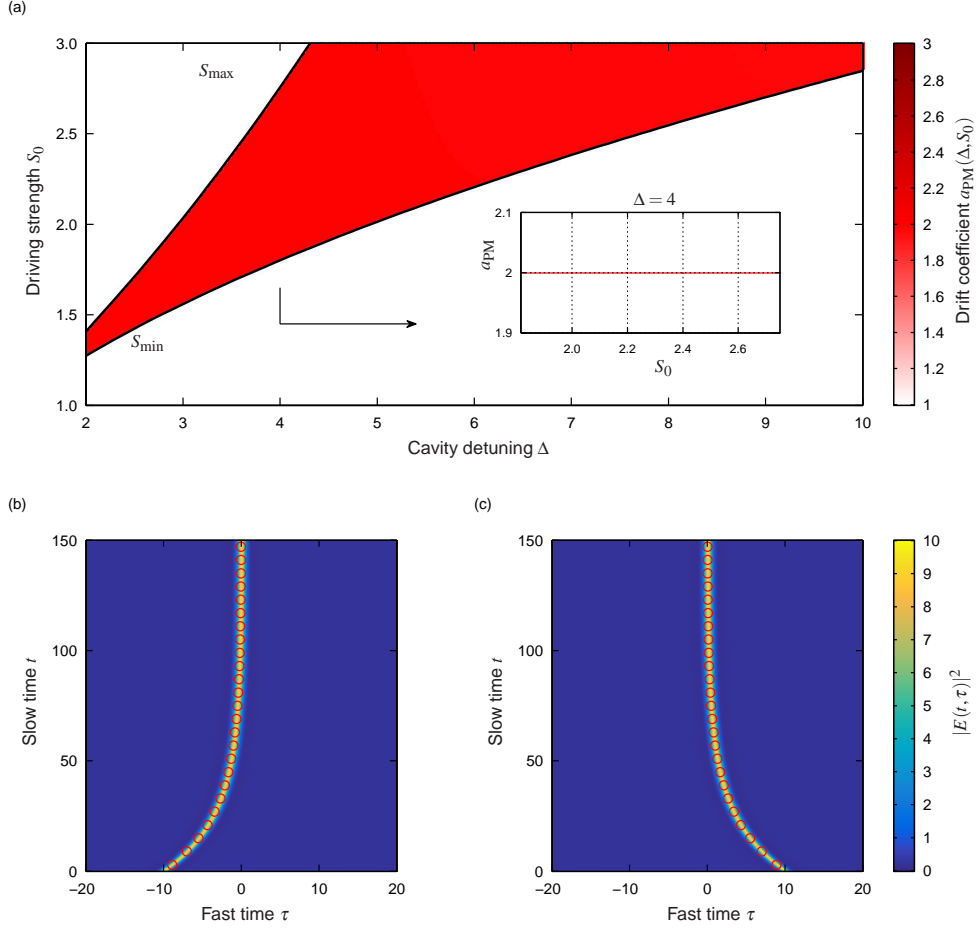


Figure 2. (a) Pseudocolor plot showing the phase drift coefficient $a_{\text{PM}}(\Delta, S_0)$ as a function of the cavity detuning Δ and driving amplitude S_0 . As can be seen, the coefficient $a_{\text{PM}}(\Delta, S_0) = 2$ for all Δ and S_0 [see also inset for the curve $a_{\text{PM}}(\Delta = 4, S_0)$ in more detail]. The black curves approximate the maximum (S_{max}) and minimum (S_{min}) driving amplitudes required for CS existence. (b) and (c) show illustrative CS dynamics in the presence of driving field phase inhomogeneities obtained via direct integration of Eq. (1). Both illustrations use $X = \Delta = 4$ and a parabolic phase profile $\phi(\tau) = -\phi_0\tau^2/\sigma^2$ with $\sigma = 10$ and $\phi_0 = 1$ rad. Red circles show theoretically predicted trajectories as described in the text. The bottom colorbar is common to (b) and (c).

sumes the constant value $a_{\text{PM}}(\Delta, S_0) = 2$ for all detunings Δ and driving amplitudes S_0 . Accordingly, the normal mode theory indeed produces the expected drift velocity $v_{\text{PM}} = 2\phi'(\tau_0)$.

A direct consequence of the result $v_{\text{PM}} = 2\phi'(\tau_0)$ is that a CS will always drift along (against) an increasing (decreasing) phase gradient. In other words, the solitons will always move towards the maxima of the phase modulation, where $\phi'(\tau) = 0$ and hence $v_{\text{PM}} = 0$. These maxima correspond to robust trapping sites: if a perturbation shifts the CS away from the maximum, the soliton will simply drift back. In contrast, whilst the CS velocity is also zero at the minima of the phase modulation, these correspond to unstable equilibria that cannot act as trapping sites in practice.

Figure 2(b) and (c) show illustrative dynamics of phase-modulation induced CS drift, obtained via numerical integration of Eq. (1); similar simulation results have been reported in a range of studies (Jang et al. 2015; Luo et al. 2015; Taheri et al. 2015; Lobanov et al. 2016). Here, Figs. 2(b) and (c) respectively show the spatiotemporal evolution of a CS initially excited at $\tau_0 = -10$ and $\tau_0 = +10$ under the influence of

a driving field with parabolic phase profile $\phi(\tau) = -\phi_0\tau^2/\sigma^2$. (For other simulation parameters, see figure caption.) As can be seen, the soliton is attracted towards – and traps to – the maximum of the phase perturbation at $\tau = 0$. Also shown as the red circles in Figs. 2(b) and (c) are the theoretically predicted CS trajectories $\tau_0(t)$ obtained by directly integrating the differential equation $d\tau_0/dt = 2\phi'(\tau)$; for the particular phase profile chosen, this yields $\tau_0(t) = \tau_0(0)\exp(-4\phi_0t/\sigma^2)$. We see very good agreement between the theoretical prediction and numerically simulated dynamics. Experimental realisations of phase modulation trapping of temporal CSs will be surveyed in Section 3.1.

2.2. Amplitude modulation

We now consider the case of a driving field that exhibits pure amplitude inhomogeneities. The underlying physics is more complicated than for the case of pure phase inhomogeneities (Hendry et al. 2018), and there is no known straightforward method to compute the CS drift velocity for amplitude inhomogeneities: the normal mode theory is necessary. To proceed, we approximate the driving field in the vicinity of the soliton as a first-order Taylor series expansion: $S(\tau) \approx S_0 + (\tau - \tau_0)S'(\tau_0)$, where $S'(\tau_0) = dS/d\tau|_{\tau_0}$. Assuming pure amplitude inhomogeneity, the perturbation $P(\tau)$ is real with $P_r(\tau) = (\tau - \tau_0)S'(\tau_0)$. Substituting this expression into Eq. (6) yields:

$$v_{\text{AM}} = \frac{d\tau_0}{dt} = a_{\text{AM}}(\Delta, S_0)S'(\tau_0), \quad (9)$$

where the coefficient $a_{\text{AM}}(\Delta, S_0)$ is given by

$$a_{\text{AM}}(\Delta, S_0) = \frac{\langle v_{0r}(\tau - \tau_0)|\tau - \tau_0 \rangle}{\left\langle v_{0r} \left| \frac{dE_{sr}}{d\tau} \right. \right\rangle + \left\langle v_{0i} \left| \frac{dE_{si}}{d\tau} \right. \right\rangle}. \quad (10)$$

Note that, in contrast to the corresponding expression for phase modulation [see Eq. (8)], the coefficient a_{AM} is obtained by projecting the *real* part of the neutral mode along a linear fast time variation, and the result is *not* multiplied by the local driving field amplitude $S_0 = S(\tau_0)$.

Figure 3(a) shows the coefficient $a_{\text{AM}}(\Delta, S_0)$ as computed for a range of detunings Δ and driving amplitudes S_0 using Eq. (8). In stark contrast with the result obtained for pure phase modulation [see Fig. 2], $a_{\text{AM}}(\Delta, S_0)$ depends nontrivially on both the detuning and the driving amplitude. We see that, for large detunings $\Delta > 3$, there exists a single “critical” driving amplitude S_c such that $a_{\text{AM}}(\Delta, S_c) = 0$. Points τ_c along the fast time that satisfy $S(\tau_c) = S_c$ correspond to stable equilibria towards which CSs are attracted – and subsequently trapped – to. Importantly, these points do not in general correspond to the extrema of the driving field: the CS may be trapped at the edge of an amplitude inhomogeneity if that is where the critical value S_c is reached (Hendry et al. 2018). It is worth noting that the extrema of the driving field are also equilibria [$S'(\tau) = 0$ implies that $v_{\text{AM}} = 0$], but these are only stable if there is no monotonic route to the critical value.

Figures 3(b)–(e) show steady-state CS profiles obtained by direct numerical simulations of Eq. (1) that illustrate the different trapping dynamics in the presence of amplitude inhomogeneities. The simulations consider a constant detuning of $\Delta = 4$ (for which the critical value $S_c = 1.98$) but different driving profiles. Figures 3(b) and

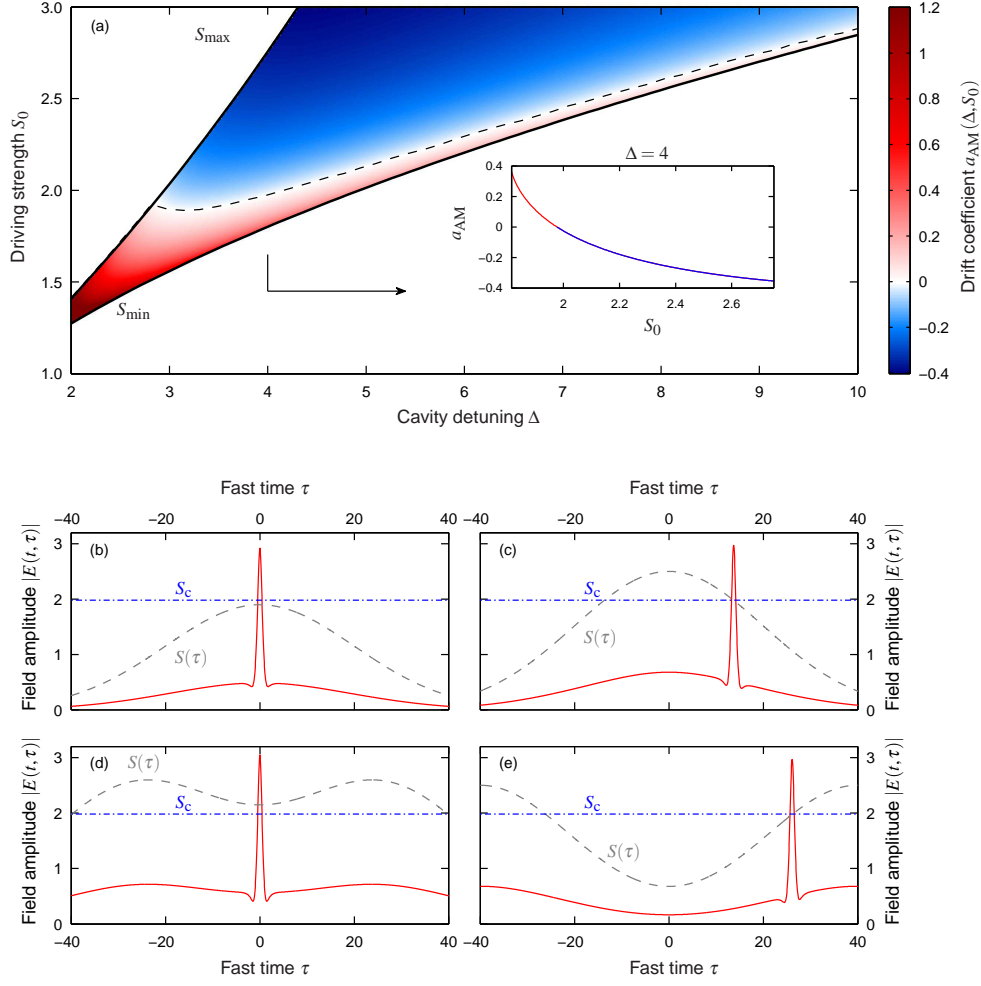


Figure 3. (a) Pseudocolor plot showing the amplitude drift coefficient $a_{AM}(\Delta, S_0)$ as a function of the cavity detuning Δ and driving amplitude S_0 . Inset shows the curve $a_{AM}(\Delta = 4, S_0)$, the black solid curves approximate the maximum (S_{max}) and minimum (S_{min}) driving amplitudes required for CS existence, and the black dashed curve highlights the points in the parameter space where $a_{AM}(\Delta, S_0) = 0$. (b)–(e) Steady-state CS profiles for different driving field amplitude profiles. (b) and (c) consider a Gaussian driving field $S(\tau) = S_g e^{-\tau^2/\sigma^2}$ with duration $\sigma = \sqrt{800}$ and peak amplitude (b) $S_g = 1.9$ and (c) $S_g = 2.5$. (d) and (e) consider a driving field that consists of a superposition of two Gaussian profiles ($\sigma = \sqrt{800}$, $S_g = 2.5$) separated from one another by (d) $\Delta\tau = 26$ and (e) $\Delta\tau = 40$. The blue dash-dotted lines indicate the critical driving amplitude $S_c \approx 1.98$. Panels (a)–(c) adapted from (Hendry et al. 2018).

(c) use a Gaussian driving field $S(\tau) = S_g e^{-\tau^2/\sigma^2}$ with two different peak amplitudes [see Figure caption for details]. When the peak amplitude $S_g < S_c$ [Fig. 3(b)], we see that the CS is attracted to the peak of the driving field – that being the point closest to the critical value S_c . In contrast, when $S_g > S_c$, we see that the CS is attracted to the edge of the driving field to a point τ_c where $S(\tau_c) = S_c$ [Fig. 3(c)]. Figures 3(d) and (e) consider a driving profile comprised of a superposition of two Gaussian pulses offset from one another [see Figure caption for details] so as to realise a local dip in the driving field. When the driving strength at the dip is greater than S_c , the CS is attracted to that point [Fig. 3(d)]. In contrast, when the driving strength at the dip is smaller than S_c , the CS is attracted to the point where the driving field attains the critical value (or a local maximum if the critical value is never attained).

2.3. Desynchronization and locking range

The analysis presented above has assumed that the phase or amplitude inhomogeneity is perfectly synchronised with the natural cavity round trip time (reciprocal of the cavity free-spectral range). This is reflected by the fact that the driving term in Eq. (1) is not dependent on the slow time t . In contrast, in the presence of desynchronisation, the externally applied inhomogeneity is advanced or delayed with respect to the intracavity field each round trip, such that $S(\tau) \rightarrow S(\tau + d \times t)$, where d represents the amount of drift. By changing into a reference frame where the pump is stationary, $\tau \rightarrow \tau - d \times t$, the LLE Eq. (1) develops a convective drift term (Coen et al. 1999; Parra-Rivas et al. 2014; Hendry et al. 2019):

$$\frac{\partial E}{\partial t} = \left[-1 + i(|E|^2 - \Delta) - d \frac{\partial}{\partial \tau} + i \frac{\partial^2}{\partial \tau^2} \right] E + S(\tau). \quad (11)$$

As discussed in (Parra-Rivas et al. 2014; Hendry et al. 2019), the pump-cavity desynchronization gives rise to a relative drift between the CS and the driving field which is in addition to the motion induced by phase or amplitude inhomogeneities. Therefore, using $a_{\text{PM}}(S_0, \Delta) = 2$, the total CS drift velocity becomes

$$v = \begin{cases} 2\phi'(\tau_0) + d & \text{for phase modulation,} \\ a_{\text{AM}}(\Delta, S_0)S'(\tau_0) + d & \text{for amplitude modulation.} \end{cases} \quad (12)$$

It should be clear that desynchronization shifts the CS locking positions to new values where $v = 0$; this shifting can also affect the number of CS configurations that can be sustained (Parra-Rivas et al. 2014; Hendry et al. 2019). Of course, if the desynchronization is too large, the equation $v = 0$ may not possess any real roots; in this case, the soliton will be unlocked, i.e., it will not be trapped to the inhomogeneity at all, but will rather circulate at its own natural repetition rate. The range of desynchronizations that can be compensated for by the inhomogeneity is known as the locking range and is given by $d_{\text{max}} = 2|\phi'(\tau_0)|_{\text{max}}$ for phase inhomogeneities and $d_{\text{max}} = |a_{\text{AM}}(\Delta, S_0)S'(\tau_0)|_{\text{max}}$ for amplitude inhomogeneities. For the sake of completeness, we present below the corresponding dimensional expressions for the locking range in terms of the frequency mismatch $\Delta f = \text{FSR} - f_{\text{H}}$, where FSR is the cavity free-spectral range (reciprocal of the natural round trip time) and f_{H} is the repetition frequency of the driving field inhomogeneity ($f_{\text{H}} \sim \text{FSR}$):

$$\Delta f_{\text{max}} \approx \begin{cases} |\beta_2|L \text{FSR}^2 |\phi'(\tau)|_{\text{max}} & \text{for phase modulation,} \\ \frac{|\beta_2|L \text{FSR}^2}{2} \sqrt{\frac{\gamma L \theta \mathcal{F}^3}{\pi^3}} |b_{\text{AM}}(\delta_0, E_{\text{in}})E'_{\text{in}}(\tau)|_{\text{max}} & \text{for amplitude modulation.} \end{cases} \quad (13)$$

Here β_2 is the group-velocity dispersion coefficient (with units of s^2m^{-1}), L is the roundtrip length of the resonator, γ is the Kerr nonlinearity coefficient (with units of $\text{W}^{-1}\text{m}^{-1}$), θ is the power transmission coefficient of the coupler used to inject the driving field into the resonator, $E_{\text{in}}(\tau)$ is the complex electric field envelope of the driving field (with units of $\text{W}^{1/2}$), \mathcal{F} is the finesse of the resonator, $\delta_0 = \pi\Delta/\mathcal{F}$ is the phase detuning between the driving field and the closest cavity resonance, and the coefficient $b_{\text{AM}}(\delta_0, E_{\text{in}}) = a_{\text{AM}}(\delta_0\mathcal{F}/\pi, E_{\text{in}}[\gamma L \theta \mathcal{F}^3/\pi^3]^{1/2})$.

Equations (13) show that that the ‘‘strength’’ of the phase modulation trapping, and

hence the attainable locking range, does not depend on the nonlinearity coefficient. This reflects the linear origins of CS motion due to phase inhomogeneities. In contrast, CS motion in the presence of amplitude inhomogeneities is intrinsically a nonlinear process (Hendry et al. 2018), and the locking range in that case is indeed found to depend on the nonlinearity coefficient γ . Because of the complicated functional form of the amplitude drift coefficient $a_{AM}(\Delta, S_0)$, it is not straightforward to quantitatively compare its strength with respect to trapping due to phase inhomogeneities. Dedicated research is needed to compare the two processes.

3. Experimental results

The section above summarised the salient theoretical details pertinent to drift and trapping of temporal Kerr CSs due to inhomogeneous driving fields. Here in this Section we review some of the key experimental results that confirm, apply, and extend upon the theoretical developments.

3.1. Phase modulation experiments

The fact that phase modulations imposed on the cavity driving beam can be used to trap CS at desired positions has been demonstrated first in the context of spatial CSs in diffractive microcavities (Pedaci et al. 2006). In the context of temporal CSs (which are at the focus of our Article), the first experimental demonstrations were reported in 2015 by Jang et al. (Jang et al. 2015). The authors excited CSs in a macroscopic (100-m-long) optical fibre ring resonator and used a 10 GHz electro-optic phase modulator to imprint a desired phase profile on the otherwise CW driving field [see Fig. 4(a)]. Figure 4(b) shows an illustrative experimental result of eight CS circulating the resonator simultaneously, each trapped to the maximum of an underlying 10 GHz sinusoidal phase modulation. It must be emphasised that, in the absence of phase modulation, the solitons would undergo spontaneous motion due to long-range interactions mediated by forward Brillouin scattering (Jang et al. 2013);

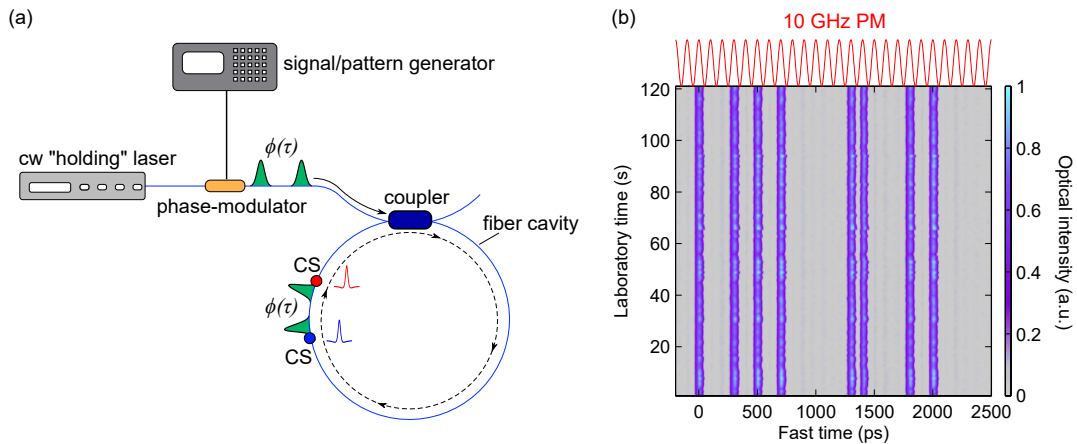


Figure 4. (a) Schematic illustration of a CS-supporting fibre ring resonator driven with a phase modulated field. (b) Experimental results, showing the trapping of eight temporal CSs to the peaks of a 10 GHz phase modulation profile (inset). Figure adapted from (Jang et al. 2015).

the fact that no such motion occurs during the two-minute experimental measurement shown in Fig. 4(b) attests to the solitons being robustly trapped to the sinusoidal phase modulation. In addition to demonstrating the general trapping potential of phase modulation, the experiments performed by Jang et al. also meticulously confirmed that, in the presence of phase modulations, the expression $v_{\text{PM}} = 2\phi'(\tau_0)$ derived above indeed provides a correct prediction for the CS drift velocity.

Following the demonstration of Jang et al., phase modulation has been widely used to trap CSs in several fibre ring resonator experiments (Wang et al. 2018b; Xu et al. 2020a), allowing e.g. for the realisation of a CS-based all-optical buffer operating at 10 GHz (Jang et al. 2016). Phase modulation has also been used in microresonator experiments to facilitate the formation of single-soliton frequency combs states that are locked to an external RF signal (Cole et al. 2018). In particular, in 2018, Cole et al. used a 9.5 mm silica wedge resonator with 22 GHz free-spectral range, driven with a CW laser phase-modulated at the fundamental FSR, to demonstrate an operating regime where only the single-soliton state is permitted – at a position that coincides with the phase modulation maximum. The authors also showed that the phase modulation trapping allows for the systematic control and stabilization of the soliton repetition rate (f_{rep}). In a very recent study, the phase modulation techniques demonstrated by Cole et al. were used to realise a frequency-stabilised coherent soliton microcomb that was subsequently demonstrated to allow for direct atomic frequency comb spectroscopy of rubidium (Stern et al. 2020).

3.2. Amplitude modulation experiments

Amplitude modulated driving fields are inherent to experiments in spatially diffractive resonators due to the impossibility of realising a perfect plane wave (rather, the driving fields tend to have broad Gaussian profiles). In contrast, in the context of dispersive resonators, CW lasers naturally provide temporally homogeneous driving fields with only minor amplitude inhomogeneities. However, as noted in the introduction of this Article, CW driving suffers from certain shortcomings that can be mitigated by employing driving fields that are not homogeneous. Numerous studies have in particular considered resonators that are driven with a train of pulses whose repetition rate is carefully synchronised to the free-spectral range of the resonator, thus ensuring that each round trip a new driving pulse is coherently added on the circulating intracavity field.

Pulsed driving has been widely used in experiments involving CSs in macroscopic fibre ring resonators (Anderson et al. 2016, 2017; Wang et al. 2018a; Nielsen et al. 2019; Xu et al. 2020a; Dong et al. 2020). These studies typically use flat-top nanosecond pulses that are much longer than the picosecond-scale CSs. Such nanosecond driving fields can be considered “quasi-CW” in that the amplitude inhomogeneity does not play any significant role for CSs residing in the flat-top portion of the field. The benefit compared to pure CW driving is, however, the possibility of reaching much greater driving amplitudes: assuming identical amplification schemes, the *peak* power attainable for a pulse train is larger than the power attainable for a CW field by a factor given by the reciprocal of the pulse train’s duty cycle. Another benefit of quasi-CW driving in the context of fibre ring resonator experiments is the fact that such driving is immune to stimulated Brillouin scattering, which is known to hinder experiments in the pure CW regime.

The use of quasi-CW pulsed driving was initially motivated by the access to larger

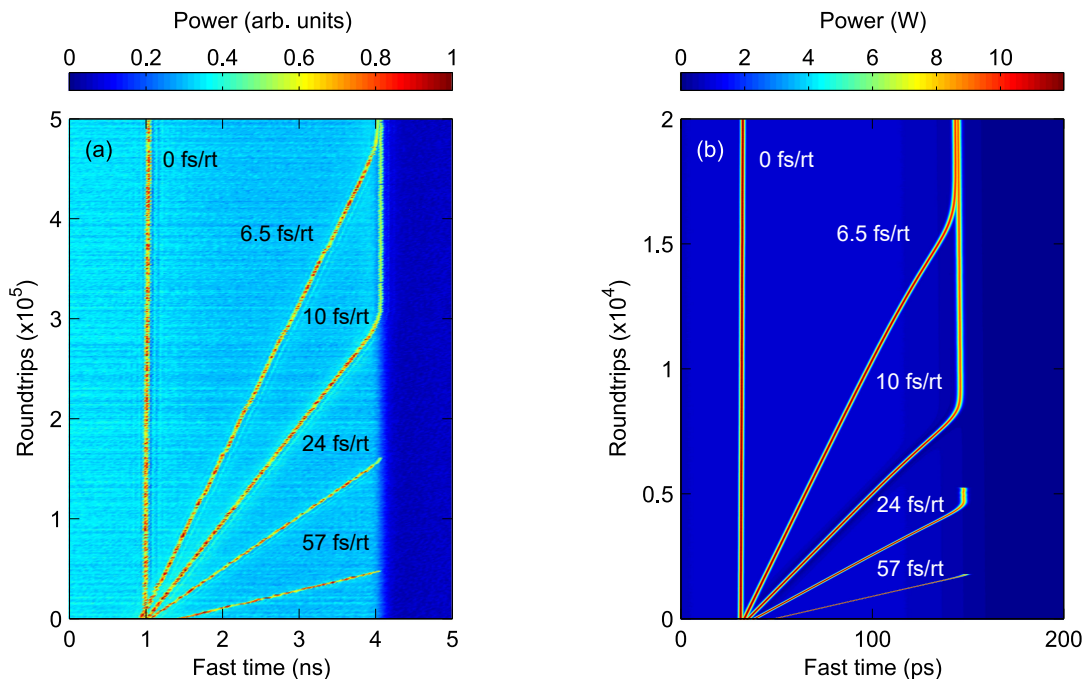


Figure 5. Assortment of (a) experimental measurements and (b) numerical simulation results for different desynchronizations that show how CSs can be trapped at the edge of amplitude inhomogeneities. The driving field is a nanosecond-scale flat-top pulse. Note that the trajectories in (a) and (b) correspond to independent realisations that have been superimposed on the same background to facilitate visualisation. Adapted from (Wang 2018).

driving powers, but it was also quickly realised that the amplitude inhomogeneity allows for CS trapping. In particular, residual desynchronization between the driving pulse train and the cavity free-spectral range causes the CSs to drift towards the leading or trailing edge of the driving field, where the solitons were found to be robustly trapped over a wide range of desynchronizations (Wang 2018; Nielsen et al. 2019). Figure 5 shows an example of such dynamics, with Figs. 5(a) and (b) showing experimental and simulated results, respectively. These results superimpose five different realisations where the desynchronization was adjusted from 0 fs per round trip to 57 fs per round trip, with a peak driving amplitude above the critical value. We clearly see how the CS can become trapped at the driving pulse edge for sufficiently small desynchronizations.

More recent experiments have also demonstrated pulsed driving to represent a viable technique to realise temporal CSs (and corresponding optical frequency combs) in high-Q microresonators. In these experiments (and in contrast to the fibre ring experiments described above), the pulses used are very short (of the order of picosecond), thus shifting truly beyond the paradigm of (quasi-)CW driving. The first demonstration of this nature was achieved by Obrzud et al., who realised CS optical frequency combs in a 1-cm-long fibre-based Fabry-Perot microresonator driven with pulses as short as 2.1 ps (Obrzud et al. 2017). The driving pulse train was generated using an electro-optic comb generation scheme (Kobayashi et al. 1972, 1988; Beha et al. 2017): CW laser light was passed through a cascaded sequence of phase and amplitude modulators and compressed into picosecond pulses by a chirped fibre-Bragg grating. It was found that temporal CSs with 200-fs-duration could form on top of the resonantly-enhanced, 2 ps intracavity pump pulses. The authors also demonstrated

that the soliton repetition rate locks to the repetition of the driving pulse train, and also examined the range of desynchronizations over which solitons can be sustained. Subsequent numerical modelling has shown that stimulated Raman scattering plays a key role in defining that range (Hendry et al. 2019).

Following the pioneering work by Obrzud et al., similar electro-optically generated pulse trains have been used to realise CSs in a range of different microresonator architectures, including silicon nitride ring resonators (Anderson et al. 2020a) and integrated silica resonators (Xu et al. 2020b). These studies have also shown that CSs can be generated when the resonator is driven at rational harmonic fractions of the cavity FSR; one such scheme has also been successfully used to realise a microresonator CS-based “astrocomb” for the detection of extra-solar planets (Obrzud et al. 2019). It is worth noting that, even though the input electro-optically generated pulse train already corresponds to a frequency comb, the CS that is generated typically has considerably shorter duration (and hence broader bandwidth) than the input. Moreover, it has been beautifully demonstrated that the soliton trapping dynamics suppress noise transfer from the input pulse train to the CS – the soliton effectively exhibits lesser timing jitter than the input pump pulse (Brasch et al. 2019; Anderson et al. 2020a). This result can be readily appreciated from Eq. (12) by first writing $a_{\text{AM}}(S_0, \Delta)S'(\tau_0) = f(\tau_0)$ to obtain

$$v = \frac{d\tau_0}{dt} = f(\tau_0) + d(t), \quad (14)$$

where the time-dependent desynchronization $d(t) = d_0 + \varepsilon(t)$ includes a constant component d_0 and a random jitter term $\varepsilon(t)$ that is assumed small ($\varepsilon \ll d_0$). Assuming further that $f(\tau_0)$ varies slowly, we may linearize the term around the average trapping position – taken to be at $\tau_0 = 0$ without loss of generality – to yield

$$v = \frac{d\tau_0}{dt} = f'(0)\tau_0 + \varepsilon(t), \quad (15)$$

where $f'(0) = df/d\tau_0|_0$ and we used the fact that $f(0) + d_0 = 0$ by virtue of $\tau_0 = 0$ being an equilibrium. Since $\tau_0 = 0$ corresponds to a stable equilibrium, we have $f'(0) < 0$. Considering harmonic jitter $\varepsilon(t) = \varepsilon_0 \exp[i\Omega t]$ and using the ansatz $\tau_0(t) = T(\Omega) \exp[i\Omega t]$, it is straightforward to derive the frequency response (Brasch et al. 2019)

$$Z(\Omega) = \frac{|T(\Omega)|^2}{|\varepsilon_0|^2} = \frac{1}{|f'(0)|^2 + \Omega^2}, \quad (16)$$

revealing a Lorentzian low-pass filter with cut-off frequency of $2|f'(0)|$. In dimensional units, the cut-off frequency $\Delta f_{\text{cutoff,AM}}$ can be written (with units of Hz) as:

$$\Delta f_{\text{cutoff,AM}} = \frac{|\beta_2|L}{2\pi} \text{FSR} \sqrt{\frac{\gamma L \theta \mathcal{F}^3}{\pi^3}} |g'(0)|, \quad (17)$$

where $g'(0)$ is the (dimensional) fast time derivative of the function $g(\tau) = b_{\text{AM}}(\delta_0, E_{\text{in}})E'_{\text{in}}(\tau)$ evaluated at the mean soliton trapping position (assumed to be $\tau = 0$) and all the other parameters are as defined in Section 2. Unexpectedly, Eq. (17) shows that a small cutoff frequency can be obtained with

parameters that are also associated with a small trapping strength [c.f. Eq. (13)]: if the soliton is only weakly coupled to the inhomogeneity, it will not react significantly to jitter in the inhomogeneity. We also note that the analysis above can be readily repeated for the case of phase modulation trapping, yielding the dimensional cutoff frequency:

$$\Delta f_{\text{cutoff,PM}} = \frac{|\beta_2|L}{\pi} \text{FSR} |\phi''(0)|. \quad (18)$$

Arguably one of the most important outcomes of the use of short pulsed driving to generate CSs is the fact that the technique has made it possible to realise CSs and corresponding frequency combs in a wider range of systems. Particularly noteworthy is the fact that pulsed driving has allowed temporal CSs to be generated and observed in a system that is fundamentally different from earlier waveguide-type resonator implementations, namely a free-space femtosecond enhancement cavity (Lilienfein et al. 2019). Specifically, considering a free-space bowtie resonator containing a 1-mm-thick sapphire plate to provide a Kerr nonlinearity, driven with a fully-stabilized mode-locked laser delivering 350 fs pulses, Lilienfein et al. demonstrated the generation of CSs as short as 37 fs. The authors’ measurements showed that, by leveraging CSs, it is possible to obtain peak-power enhancements an order of magnitude larger than previously demonstrated in femtosecond enhancement cavities with similar pulse durations. Compounded by the solitons’ noise suppression characteristics, the results underline the potential usefulness of temporal CSs in an entirely new spectrum of applications (Brasch et al. 2019), including high-order harmonic generation (Gohle et al. 2005) and photoemission spectroscopy (Saule et al. 2019).

4. Conclusions and future outlook

The use of driving fields with phase or amplitude inhomogeneities offers a number of advantages for the study and application of temporal Kerr cavity solitons, including the ability to implement robust soliton trapping and control schemes. In this Article, we have reviewed the salient theoretical descriptions of CS dynamics in the presence of inhomogeneous driving fields, and surveyed relevant experimental literature.

We envisage that inhomogeneous driving fields will continue to gain in popularity in CS-related studies, stimulating significant future research. For example, the fact that pulsed driving gives access to very large (peak) power levels is likely to further expand the systems in which CSs and related frequency combs can be generated, paving the way for new applications. The knowledge generated over the past few years also provides an avenue for optimising a given CS control parameter (such as locking range or nonlinear filtering bandwidth), which is likely to allow inhomogeneous driving fields to further enhance the performance of existing applications. In this context, it is worth noting that studies so far have focussed on phase or amplitude inhomogeneities in isolation: we expect that judiciously engineered combination of the two is likely to be key for future optimisation.

It is also important to note that our understanding of CS control and trapping with driving field inhomogeneities is so far built around situations where higher-order effects – such as stimulated Raman scattering or higher-order dispersion – are negligible. Considerable research is needed to understand how the underlying physics change when higher-order effects play a significant role. For example, recent experiments have

shown signatures of CSs that can exist under conditions of weak normal dispersion driving (Li et al. 2020; Anderson et al. 2020b); in this regime, third-order dispersion plays a dominant role and is expected to alter the CS trapping dynamics. Similarly, the response of CSs to driving field inhomogeneities in systems with multiple interacting spatial or polarization mode families (Lucas et al. 2018; Nielsen et al. 2019; Xu et al. 2020a) – or coupled cavity configurations (Xue et al. 2019; Kim et al. 2019; Helgason et al. 2020) – represents an interesting area of further research. Finally, we envisage that the phase and amplitude trapping of other localized structures – such as dark solitons (Xue et al. 2015; Fülöp et al. 2018) or platicons (Lobanov et al. 2015) – that can manifest themselves in Kerr resonators is also likely to draw research attention in the coming years.

Acknowledgements

We acknowledge financial support from the Marsden Fund and the Rutherford Discovery Fellowships of the Royal Society of New Zealand. We would also like to thank Dr Yadong Wang for providing data and codes to plot Figure 5 and Mr Ian Hendry for useful discussions.

References

- Ackemann, T., Firth, W., and Oppo, G.-L. (2009). Fundamentals and Applications of Spatial Dissipative Solitons in Photonic Devices. *Adv. Atom. Mol. Opt. Phys.* 57:323.
- Akhmediev, N. and Ankiewicz, A. (2008). *Dissipative Solitons: From Optics to Biology and Medicine*, volume 751 of *Lecture Notes in Physics*. Springer Berlin Heidelberg, Berlin, Heidelberg.
- Anderson, M., Leo, F., Coen, S., Erkintalo, M., and Murdoch, S. G. (2016). Observations of spatiotemporal instabilities of temporal cavity solitons. *Optica*, 3(10):1071.
- Anderson, M., Wang, Y., Leo, F., Coen, S., Erkintalo, M., and Murdoch, S. G. (2017). Coexistence of Multiple Nonlinear States in a Tristable Passive Kerr Resonator. *Phys. Rev. X*, 7(3):031031.
- Anderson, M. H., Bouchand, R., Liu, J., Weng, W., Obrzud, E., Herr, T., and Kippenberg, T. J. (2020a). Photonic chip-based resonant supercontinuum. *arXiv:1909.00022 [physics]*.
- Anderson, M. H., Lihachev, G., Weng, W., Liu, J., and Kippenberg, T. J. (2020b). Zero-dispersion Kerr solitons in optical microresonators. *arXiv:2007.14507 [physics]*.
- Bao, C., Zhang, L., Matsko, A., Yan, Y., Zhao, Z., Xie, G., Agarwal, A. M., Kimerling, L. C., Michel, J., Maleki, L., and Willner, A. E. (2014). Nonlinear conversion efficiency in Kerr frequency comb generation. *Opt. Lett.*, 39(21):6126–6129.
- Barland, S., Tredicce, J. R., Brambilla, M., Lugiato, L. A., Balle, S., Giudici, M., Maggipinto, T., Spinelli, L., Tissoni, G., Knödl, T., Miller, M., and Jäger, R. (2002). Cavity solitons as pixels in semiconductor microcavities. *Nature*, 419(6908):699–702.
- Beha, K., Cole, D. C., Del’Haye, P., Coillet, A., Diddams, S. A., and Papp, S. B. (2017). Electronic synthesis of light. *Optica*, 4(4):406–411.
- Brasch, V., Geiselmann, M., Herr, T., Lihachev, G., Pfeiffer, M. H. P., Gorodetsky, M. L., and Kippenberg, T. J. (2016). Photonic chip-based optical frequency comb using soliton Cherenkov radiation. *Science*, 351(6271):357–360.
- Brasch, V., Obrzud, E., Lecomte, S., and Herr, T. (2019). Nonlinear filtering of an optical pulse train using dissipative Kerr solitons. *Optica*, 6(11):1386–1393.
- Coen, S., Tlidi, M., Emplit, P., and Haelterman, M. (1999). Convection versus Dispersion in Optical Bistability. *Phys. Rev. Lett.*, 83(12):2328–2331.

- Cole, D. C., Stone, J. R., Erkintalo, M., Yang, K. Y., Yi, X., Vahala, K. J., and Papp, S. B. (2018). Kerr-microresonator solitons from a chirped background. *Optica*, 5(10):1304–1310.
- Dong, X., Yang, Q., Spiess, C., Bucklew, V. G., and Renninger, W. H. (2020). Stretched-Pulse Soliton Kerr Resonators. *Phys. Rev. Lett.*, 125(3):033902.
- Dutt, A., Joshi, C., Ji, X., Cardenas, J., Okawachi, Y., Luke, K., Gaeta, A. L., and Lipson, M. (2018). On-chip dual-comb source for spectroscopy. *Science Advances*, 4(3):e1701858.
- Firth, W. J. and Scroggie, A. J. (1996). Optical Bullet Holes: Robust Controllable Localized States of a Nonlinear Cavity. *Phys. Rev. Lett.*, 76(10):1623–1626.
- Fülöp, A., Mazur, M., Lorences-Riesgo, A., Helgason, Ó. B., Wang, P.-H., Xuan, Y., Leaird, D. E., Qi, M., Andrekson, P. A., Weiner, A. M., and Torres-Company, V. (2018). High-order coherent communications using mode-locked dark-pulse Kerr combs from microresonators. *Nature Commun.*, 9(1):1–8.
- Gohle, C., Udem, T., Herrmann, M., Rauschenberger, J., Holzwarth, R., Schuessler, H. A., Krausz, F., and Hänsch, T. W. (2005). A frequency comb in the extreme ultraviolet. *Nature*, 436(7048):234–237.
- Guo, H., Karpov, M., Lucas, E., Kordts, A., Pfeiffer, M. H. P., Brasch, V., Lihachev, G., Lobanov, V. E., Gorodetsky, M. L., and Kippenberg, T. J. (2017). Universal dynamics and deterministic switching of dissipative Kerr solitons in optical microresonators. *Nature Phys.*, 13(1):94–102.
- Haelterman, M., Trillo, S., and Wabnitz, S. (1992). Dissipative modulation instability in a nonlinear dispersive ring cavity. *Opt. Commun.*, 91(5–6):401–407.
- Helgason, Ó. B., Arteaga-Sierra, F. R., Ye, Z., Twayana, K., Andrekson, P. A., Karlsson, M., Schröder, J., and Torres-Company, V. (2020). Dissipative Kerr solitons in photonic molecules. *arXiv:2007.02608 [nltn, physics:physics]*.
- Hendry, I., Chen, W., Wang, Y., Garbin, B., Javaloyes, J., Oppo, G.-L., Coen, S., Murdoch, S. G., and Erkintalo, M. (2018). Spontaneous symmetry breaking and trapping of temporal Kerr cavity solitons by pulsed or amplitude-modulated driving fields. *Phys. Rev. A*, 97(5):053834.
- Hendry, I., Garbin, B., Murdoch, S. G., Coen, S., and Erkintalo, M. (2019). Impact of desynchronization and drift on soliton-based Kerr frequency combs in the presence of pulsed driving fields. *Phys. Rev. A*, 100(2):023829.
- Herr, T., Brasch, V., Jost, J. D., Wang, C. Y., Kondratiev, N. M., Gorodetsky, M. L., and Kippenberg, T. J. (2014). Temporal solitons in optical microresonators. *Nature Photon.*, 8(2):145–152.
- Jang, J. K., Erkintalo, M., Coen, S., and Murdoch, S. G. (2015). Temporal tweezing of light through the trapping and manipulation of temporal cavity solitons. *Nature Commun.*, 6(1):7370.
- Jang, J. K., Erkintalo, M., Murdoch, S. G., and Coen, S. (2013). Ultraweak long-range interactions of solitons observed over astronomical distances. *Nature Photon.*, 7(8):657–663.
- Jang, J. K., Erkintalo, M., Schröder, J., Eggleton, B. J., Murdoch, S. G., and Coen, S. (2016). All-optical buffer based on temporal cavity solitons operating at 10 Gb/s. *Opt. Lett.*, 41(19):4526.
- Jang, J. K., Klenner, A., Ji, X., Okawachi, Y., Lipson, M., and Gaeta, A. L. (2018). Synchronization of coupled optical microresonators. *Nature Photon.*, 12(11):688–693.
- Joshi, C., Jang, J. K., Luke, K., Ji, X., Miller, S. A., Klenner, A., Okawachi, Y., Lipson, M., and Gaeta, A. L. (2016). Thermally controlled comb generation and soliton modelocking in microresonators. *Opt. Lett.*, 41(11):2565–2568.
- Karpov, M., Pfeiffer, M. H. P., Guo, H., Weng, W., Liu, J., and Kippenberg, T. J. (2019). Dynamics of soliton crystals in optical microresonators. *Nature Phys.*, 15(10):1071–1077.
- Kelley, C. T. (2003). *Solving Nonlinear Equations with Newton’s Method*. Fundamentals of Algorithms. Society for Industrial and Applied Mathematics.
- Kim, B. Y., Okawachi, Y., Jang, J. K., Yu, M., Ji, X., Zhao, Y., Joshi, C., Lipson, M., and Gaeta, A. L. (2019). Turn-key, high-efficiency Kerr comb source. *Opt. Lett.*, 44(18):4475–4478.

- Kippenberg, T. J., Gaeta, A. L., Lipson, M., and Gorodetsky, M. L. (2018). Dissipative Kerr solitons in optical microresonators. *Science*, 361(6402):eaan8083.
- Kobayashi, T., Sueta, T., Cho, Y., and Matsuo, Y. (1972). High-repetition-rate optical pulse generator using a Fabry-Perot electro-optic modulator. *Appl. Phys. Lett.*, 21(8):341–343.
- Kobayashi, T., Yao, H., Amano, K., Fukushima, Y., Morimoto, A., and Sueta, T. (1988). Optical pulse compression using high-frequency electrooptic phase modulation. *IEEE Journal of Quantum Electronics*, 24(2):382–387.
- Leo, F., Coen, S., Kockaert, P., Gorza, S.-P., Emplit, P., and Haelterman, M. (2010). Temporal cavity solitons in one-dimensional Kerr media as bits in an all-optical buffer. *Nature Photon.*, 4(7):471–476.
- Leo, F., Gelens, L., Emplit, P., Haelterman, M., and Coen, S. (2013). Dynamics of one-dimensional Kerr cavity solitons. *Opt. Express*, 21(7):9180–9191.
- Li, Z., Xu, Y., Coen, S., Murdoch, S. G., and Erkintalo, M. (2020). Experimental observations of bright dissipative cavity solitons and their collapsed snaking in a Kerr resonator with normal dispersion driving. *Optica*, 7(9):1195–1203.
- Lilienfein, N., Hofer, C., Högner, M., Saule, T., Trubetskov, M., Pervak, V., Fill, E., Riek, C., Leitenstorfer, A., Limpert, J., Krausz, F., and Pupeza, I. (2019). Temporal solitons in free-space femtosecond enhancement cavities. *Nature Photon.*, 13(3):214–218.
- Lobanov, V. E., Lihachev, G., Kippenberg, T. J., and Gorodetsky, M. L. (2015). Frequency combs and platons in optical microresonators with normal GVD. *Opt. Express*, 23(6):7713–7721.
- Lobanov, V. E., Lihachev, G. V., Pavlov, N. G., Cherenkov, A. V., Kippenberg, T. J., and Gorodetsky, M. L. (2016). Harmonization of chaos into a soliton in Kerr frequency combs. *Opt. Express*, 24(24):27382–27394.
- Lucas, E., Lihachev, G., Bouchand, R., Pavlov, N. G., Raja, A. S., Karpov, M., Gorodetsky, M. L., and Kippenberg, T. J. (2018). Spatial multiplexing of soliton microcombs. *Nature Photon.*, 12(11):699–705.
- Lugiato, L. A. and Lefever, R. (1987). Spatial Dissipative Structures in Passive Optical Systems. *Phys. Rev. Lett.*, 58(21):2209–2211.
- Luo, K., Jang, J. K., Coen, S., Murdoch, S. G., and Erkintalo, M. (2015). Spontaneous creation and annihilation of temporal cavity solitons in a coherently driven passive fiber resonator. *Opt. Lett.*, 40(16):3735–3738.
- Maggipinto, T., Brambilla, M., Harkness, G. K., and Firth, W. J. (2000). Cavity solitons in semiconductor microresonators: Existence, stability, and dynamical properties. *Phys. Rev. E*, 62(6):8726–8739.
- Marin-Palomo, P., Kemal, J. N., Karpov, M., Kordts, A., Pfeifle, J., Pfeiffer, M. H. P., Trocha, P., Wolf, S., Brasch, V., Anderson, M. H., Rosenberger, R., Vijayan, K., Freude, W., Kippenberg, T. J., and Koos, C. (2017). Microresonator-based solitons for massively parallel coherent optical communications. *Nature*, 546(7657):274.
- Nielsen, A. U., Garbin, B., Coen, S., Murdoch, S. G., and Erkintalo, M. (2019). Coexistence and interactions between nonlinear states with different polarizations in a monochromatically driven passive Kerr resonator. *Phys. Rev. Lett.*, 123(1):013902.
- Obrzud, E., Lecomte, S., and Herr, T. (2017). Temporal solitons in microresonators driven by optical pulses. *Nature Photon.*, 11(9):600.
- Obrzud, E., Rainer, M., Harutyunyan, A., Anderson, M. H., Liu, J., Geiselmann, M., Chazelas, B., Kundermann, S., Lecomte, S., Ceconi, M., Ghedina, A., Molinari, E., Pepe, F., Wildi, F., Bouchy, F., Kippenberg, T. J., and Herr, T. (2019). A microphotonic astrocomb. *Nature Photon.*, 13(1):31–35.
- Parra-Rivas, P., Gomila, D., Matías, M. A., Colet, P., and Gelens, L. (2014). Effects of inhomogeneities and drift on the dynamics of temporal solitons in fiber cavities and microresonators. *Opt. Express*, 22(25):30943–30954.
- Pasquazi, A., Peccianti, M., Razzari, L., Moss, D. J., Coen, S., Erkintalo, M., Chembo, Y. K., Hansson, T., Wabnitz, S., Del’Haye, P., Xue, X., Weiner, A. M., and Morandotti, R. (2018). Micro-combs: A novel generation of optical sources. *Phys. Rep.*, 729:1–81.

- Pedaci, F., Genevet, P., Barland, S., Giudici, M., and Tredicce, J. R. (2006). Positioning cavity solitons with a phase mask. *Applied Physics Letters*, 89(22):221111.
- Riemensberger, J., Lukashchuk, A., Karpov, M., Weng, W., Lucas, E., Liu, J., and Kippenberg, T. J. (2020). Massively parallel coherent laser ranging using a soliton microcomb. *Nature*, 581(7807):164–170.
- Saule, T., Heinrich, S., Schötz, J., Lilienfein, N., Högnér, M., deVries, O., Plötner, M., Weitenberg, J., Esser, D., Schulte, J., Russbueldt, P., Limpert, J., Kling, M. F., Kleineberg, U., and Pupeza, I. (2019). High-flux ultrafast extreme-ultraviolet photoemission spectroscopy at 18.4 MHz pulse repetition rate. *Nature Commun.*, 10(1):458.
- Spencer, D. T., Drake, T., Briles, T. C., Stone, J., Sinclair, L. C., Fredrick, C., Li, Q., Westly, D., Ilic, B. R., Bluestone, A., Volet, N., Komljenovic, T., Chang, L., Lee, S. H., Oh, D. Y., Suh, M.-G., Yang, K. Y., Pfeiffer, M. H. P., Kippenberg, T. J., Norberg, E., Theogarajan, L., Vahala, K., Newbury, N. R., Srinivasan, K., Bowers, J. E., Diddams, S. A., and Papp, S. B. (2018). An optical-frequency synthesizer using integrated photonics. *Nature*, 557(7703):81–85.
- Stern, L., Stone, J. R., Kang, S., Cole, D. C., Suh, M.-G., Fredrick, C., Newman, Z., Vahala, K., Kitching, J., Diddams, S. A., and Papp, S. B. (2020). Direct Kerr frequency comb atomic spectroscopy and stabilization. *Science Advances*, 6(9):eaax6230.
- Suh, M.-G. and Vahala, K. J. (2018). Soliton microcomb range measurement. *Science*, 359(6378):884–887.
- Suh, M.-G., Yang, Q.-F., Yang, K. Y., Yi, X., and Vahala, K. J. (2016). Microresonator soliton dual-comb spectroscopy. *Science*, 354(6312):600–603.
- Suh, M.-G., Yi, X., Lai, Y.-H., Leifer, S., Grudinin, I. S., Vasisht, G., Martin, E. C., Fitzgerald, M. P., Doppmann, G., Wang, J., Mawet, D., Papp, S. B., Diddams, S. A., Beichman, C., and Vahala, K. (2019). Searching for exoplanets using a microresonator astrocomb. *Nature Photon.*, 13(1):25–30.
- Taheri, H., Eftekhari, A. A., Wiesenfeld, K., and Adibi, A. (2015). Soliton Formation in Whispering-Gallery-Mode Resonators via Input Phase Modulation. *IEEE Photonics Journal*, 7(2):1–9.
- Trocha, P., Karpov, M., Ganin, D., Pfeiffer, M. H. P., Kordts, A., Wolf, S., Krockenberger, J., Marin-Palomo, P., Weimann, C., Randel, S., Freude, W., Kippenberg, T. J., and Koos, C. (2018). Ultrafast optical ranging using microresonator soliton frequency combs. *Science*, 359(6378):887–891.
- Wabnitz, S. (1993). Suppression of interactions in a phase-locked soliton optical memory. *Opt. Lett.*, 18(8):601–603.
- Wang, Y. (2018). *Temporal Cavity Soliton Dynamics in Passive Kerr Resonators*. Doctoral Thesis, The University of Auckland.
- Wang, Y., Anderson, M., Coen, S., Murdoch, S. G., and Erkintalo, M. (2018a). Stimulated Raman Scattering Imposes Fundamental Limits to the Duration and Bandwidth of Temporal Cavity Solitons. *Phys. Rev. Lett.*, 120(5):053902.
- Wang, Y., Garbin, B., Leo, F., Coen, S., Erkintalo, M., and Murdoch, S. G. (2018b). Addressing temporal Kerr cavity solitons with a single pulse of intensity modulation. *Opt. Lett.*, 43(13):3192–3195.
- Wang, Y., Leo, F., Fatome, J., Erkintalo, M., Murdoch, S. G., and Coen, S. (2017). Universal mechanism for the binding of temporal cavity solitons. *Optica*, 4(8):855–863.
- Xu, G., Nielsen, A., Garbin, B., Hill, L., Oppo, G.-L., Fatome, J., Murdoch, S. G., Coen, S., and Erkintalo, M. (2020a). Spontaneous symmetry breaking of dissipative optical solitons in a two-component Kerr resonator. *arXiv:2008.13776 [physics]*.
- Xu, Y., Lin, Y., Nielsen, A., Hendry, I., Coen, S., Erkintalo, M., Ma, H., Murdoch, S. G., (2020b). Harmonic and rational harmonic driving of microresonator soliton frequency combs. *Optica*, 7(8):940–946.
- Xue, X., Wang, P.-H., Xuan, Y., Qi, M., and Weiner, A. M. (2017). Microresonator Kerr frequency combs with high conversion efficiency. *Laser & Photonics Reviews*, 11(1):1600276.
- Xue, X., Xuan, Y., Liu, Y., Wang, P.-H., Chen, S., Wang, J., Leaird, D. E., Qi, M., and Weiner,

- A. M. (2015). Mode-locked dark pulse Kerr combs in normal-dispersion microresonators. *Nature Photon.*, 9(9):594–600.
- Xue, X., Zheng, X., and Zhou, B. (2019). Super-efficient temporal solitons in mutually coupled optical cavities. *Nature Photon.*, 13(9):616–622.
- Yi, X., Yang, Q.-F., Yang, K. Y., Suh, M.-G., and Vahala, K. (2015). Soliton frequency comb at microwave rates in a high-Q silica microresonator. *Optica*, 2(12):1078.